SAP30BP interacts with RBM17/SPF45 to promote splicing in a subset of human short introns

Kazuhiro Fukumura[1]*, Luca Sperotto[2,3], Stefanie Seuß[2,3], Hyun-Seo Kang[2,3], Rei Yoshimoto[4], Michael Sattler[2,3], and Akila Mayeda[1,5]*

[1]Division of Gene Expression Mechanism, Center for Medical Science, Fujita Health University, Toyoake, Aichi 470-1192, Japan
[2]Institute of Structural Biology, Helmholtz Zentrum München, 85764 Neuherberg, Germany
[3]Bavarian NMR Center, School of Natural Sciences, Technical University of Munich, 85748 Garching, Germany
[4]Department of Applied Biological Sciences, Faculty of Agriculture, Setsunan University, Hirakata, Osaka 673-0101, Japan

[5]Lead contact
*Correspondences: fukumura@fujita-hu.ac.jp (K.F.), mayeda@fujita-hu.ac.jp (A.M.)

Keywords: Pre-mRNA splicing, short intron, poly-pyrimidine tract, RBM17 (SPF45), SAB30BP, U2AF heterodimer, U2 snRNP, SF3B1 (SF3b155), U2AF-homology motif (UHM), UHM-ligand motif (ULM)

SUMMARY

Human pre-mRNA splicing requires the removal of introns with highly variable lengths, from tens to over a million nucleotides. Therefore, mechanisms of intron recognition and splicing are likely not universal. Recently, we reported that splicing in a subset of human short introns with truncated polypyrimidine tracts depends on RBM17 (SPF45), instead of the canonical splicing factor U2AF heterodimer. Here, we demonstrate that SAP30BP, a factor previously implicated in transcriptional control, is an essential splicing cofactor for RBM17. *In vitro* binding and NMR analyses demonstrate that a U2AF-homology motif (UHM) in RBM17 binds directly to a newly identified UHM-ligand motif (ULM) in SAP30BP. We show that this RBM17–SAP30BP interaction is required to specifically recruit RBM17 to phosphorylated SF3B1 (SF3b155), a U2 snRNP component in active spliceosomes. We propose a unique mechanism for splicing in a subset of short introns, in which SAP30BP guides RBM17 in the assembly of active spliceosomes.

INTRODUCTION

Human pre-mRNA introns vary extensively in length, ranging from under fifty to over a million nucleotides (nt) (Piovesan et al., 2015). On the other hand, the known molecular mechanism of pre-mRNA splicing was biochemically established using ideal model pre-mRNAs with a single relatively short intron. The common model substrates are human β-globin pre-mRNA with 158-nt intron and adenovirus 2 major late (AdML) pre-mRNA with 231-nt intron, which are efficiently spliced *in vitro* and *in cellulo* (protocols in Mayeda and Krainer, 2012; López-Mejía and Tazi, 2012).

Therefore, the known essential *cis*-acting splicing signals and the binding *trans*-acting splicing factors in the early spliceosomal complex were analyzed with such ideal model pre-mRNAs; i.e., the 5′ splice site, the branch-site sequence, and the poly-pyrimidine tract (PPT) followed by the 3′ splice site that are bound by U1 snRNP, U2 snRNP and U2AF2–U2AF1 ($U2AF^{65}$–$U2AF^{35}$), respectively (reviewed in Will and Lührmann, 2011; Kastner et al., 2019). This aspect was realized by our recent

discovery; i.e., a subset of human short introns with truncated PPTs are spliced out by RBM17 (SPF45), but not by the known U2AF heterodimer (Fukumura et al., 2021).

In this distinct splicing mechanism, the U2AF-homology motif (UHM) of RBM17 competes out that of U2AF2 for binding to the UHM-ligand motif (ULM) of SF3B1 (SF3b155) in the U2 snRNP (Figure 1A). Our nuclear magnetic resonance (NMR) spectroscopy data revealed that neither the UHM domain nor the G-patch motif of RBM17 binds the truncated PPT *in vitro*, while both of these are critical for RBM17 to be localized on the truncated PPT and for eventual RBM17-dependent splicing *in cellulo* (Fukumura et al., 2021). Therefore, we postulate that the recruitment of RBM17 in the functional position on short introns requires an additional protein factor ('Unknown factor X' in Figure 1A).

Intriguingly, three previous studies have implicated SAP30BP as a promising potential RBM17-interacting cofactor: (i) SAP30BP (HCNGP) was detected as a non-snRNP protein in human spliceosomal A complexes (Behzadnia et al., 2007), (ii) the fruit fly homologs of SAP30BP and RBM17 were detected in spliceosomal complexes formed on a short intron (62-nt) but not on a long intron (147-nt) (Herold et al., 2009), and (iii) yeast two-hybrid protein interaction assays showed that RBM17 can interact with SAP30BP (Table S3 in Hegele et al., 2012).

Here we demonstrate that SAP30BP is a functional partner in RBM17-dependent splicing. Interestingly, the binding of SAP30BP to RBM17 is important prior to the RBM17 interaction with phosphorylated SF3B1, a component of active U2 snRNP.

RESULTS

siRNA-knockdown of SAP30BP represses endogenous RBM17-dependent splicing

To test the functional role of SAP30BP in RBM17-dependent splicing, we performed siRNA-mediated depletions of SAP30B, RBM17 (positive control), and SAP30 (negative control) in HeLa cells (Figure 1B). Total RNAs were then analyzed by RT–PCR to examine RBM17-dependent splicing activity of the endogenous pre-mRNAs targeting the 56-nt (intron 7 of *HNRNPH1*), the 71-nt (intron 17 of *EML3*), the 74-nt (intron 13 of *MUS81*), and the 76-nt (intron 5 of *MTA1*); which were all previously

identified as RBM17-dependently spliced pre-mRNAs (Fukumura et al., 2021). These short introns were effectively repressed not only in RBM17-depleted cells but also in SAP30BP-depleted cells, whereas such splicing repression was not observed with the control pre-mRNA (366-nt intron 5 of *DUSP1*; Figure 1C). These data suggest that SAP30BP plays a key role in RBM17-dependent splicing but not in U2AF-dependent conventional splicing.

SAP30BP and RBM17 are critical to splice out many short introns

To test whether SAP30BP is generally required for RBM17-dependent splicing, we performed whole-transcriptome sequencing (RNA-Seq) analysis in either RBM17-deficient or SAP30BP-deficient HeLa cells. The sequencing reads were mapped to the human genome reference sequence, and we identified total 2077 events of intron retention (i.e., splicing inhibition) in which 326 events overlapped with knockdown of RBM17 and SAP30BP; namely, more than half of the retained introns in RBM17-deficient cells were shared with those in SAP30BP-deficient cells (Figure 2A; see Supplementary Table S1 for the list of all 326 introns). Notably, the length distribution of these retained-introns in RBM17-depleted and SAP30BP-depleted cells is strongly biased towards shorter lengths compared to all introns in general (Figure 2B).

Together, these results demonstrate that RBM17 and SAP30BP cooperatively and ubiquitously function for efficient splicing of a distinct population of pre-mRNAs with short introns.

RBM17 and SAP30BP cooperate in RBM17-dependent splicing

We recently demonstrated that a truncated PPT is a responsive *cis*-element for RBM17-dependent splicing. Therefore, we examined whether the SAP30BP-dependency is also related to the truncated PPT.

First, we confirmed that RBM17-dependent splicing, as well as SAP30BP-dependent splicing, is recapitulated in ectopically expressed mini-genes including short introns as in the corresponding endogenous genes (Figure 1C). The splicing in HNRNPH1 (56-nt intron) and EML3 (71-nt intron) pre-mRNAs was repressed by depletion of either RBM17 or SAP30BP, whereas splicing of the control adenovirus 2 major late (AdML) pre-mRNA (231-nt intron) was unaffected (Supplementary Figure

S1A).

Next, we proceeded to analyze the role of the PPT using ectopically expressed chimeric mini-genes. Regarding the RBM17-dependency on the chimeric HNRNPH1 pre-mRNAs (the intronic fragments were replaced with those from control AdML pre-mRNA), we observed results consistent with our recent report (Supplementary Figure S1B, C ;Fukumura et al., 2021); i.e., (i) the replacement of the truncated 13-nt PPT of HNRNPH1 with the conventional 25-nt PPT of AdML switched the pre-mRNA to RBM17-independent splicing (AdML PPT25; Supplementary Figure S1B), (ii) the truncation of this AdML PPT to 13-nt regained RBM17-dependency (AdML PPT13), and (iii) the expansion of the upstream intron region between the 5′ splice site and the branch site with a short HNRNPH1 PPT retained RBM17 dependency (AdML 5′MT). Remarkably, knockdown of SAP30BP exactly follows the above RBM17-dependency (Supplementary Figure S1B). All these results were also recapitulated with another chimeric EML3 pre-mRNA with truncated 12-nt PPT (Supplementary Figure S1C). Our global PPT length analysis of the retained introns in SAP30BP-knockdown cells showed similar PPT length distribution as those in RBM17-knockdown cells (Supplementary Figure S2).

We conclude that RBM17 and SAP30BP act cooperatively in RBM17-dependent splicing, specifically for short introns with truncated PPTs.

RBM17 binds to SAP30BP through UHM–ULM interaction

The cooperation of RBM17 and SAP30BP in splicing of pre-mRNAs with short introns suggest a direct interaction of these two factors *in cellulo*. To test this hypothesis, HeLa cells were co-transfected with Myc-SAP30BP and FLAG-RBM17 expression plasmids, immunoprecipitated with anti-Flag antibody, and the co-precipitated proteins were detected by anti-Flag or anti-Myc antibody. The immunoblot showed that RBM17 bound to SAP30BP and SF3B1 (positive control), but not to SAP30 (negative control), suggesting the formation of a RBM17–SAP30BP complex (Figure 3A).

Next, we investigated which regions in RBM17 and SAP30BP are required for complex formation. We prepared *E. coli* recombinant glutathione S-transferase (GST)-fusion proteins of RBM17, SAP30BP, and various deletion and mutation constructs (Figures 3B, 3D; upper schemata). Our GST pull-down assays revealed

that deletion of the N-terminal region, including or excluding the G-patch motif (RBM17/ΔNΔG, RBM17ΔN), greatly reduced binding to SAP30BP (lower panel). While deletion of the G-patch motif alone (RBM17/ΔG) did not affect the SAP30BP interaction. Deletion of either half of the N-terminal domain (RBM17/ΔN1, RBM17/ΔN2) strongly reduced binding to SAP30BP indicating that the complete N-terminal domain contributes to the SAP30BP interaction (Supplementary Figure S3). However, the complete or middle part of the N-terminal domain alone (RBM17/N, RBM17/N3) showed no binding to SAP30BP (Supplementary Figure S3). The C-terminal region of RBM17 harbors the UHM domain, and a D319K mutation in the UHM (RBM17/UHMmt), which inhibits ULM binding (Fukumura et al., 2021), greatly reduced the SAP30BP interaction. These data suggest that a ULM–UHM interaction is important for the complex formation. Together, we conclude that the RBM17–UHM is essential to interact with SAP30BP and that the N-terminal domain of RBM17 might additionally contribute to SAP30BP binding.

Consistent with the RBM17–UHM-mediated binding of SAP30BP, we indeed identified a ULM sequence in the C-terminal region of SAP30BP, which could mediate the interaction with the RBM17–UHM (Figure 3C; Figure 3D, upper schemata). Deletion of the C-terminal region of SAP30BP alone or both N- and C-terminal regions (SAP30BP/ΔC, SAP30BP/ΔNΔC) abrogated binding to RBM17, while deletion of the N-terminal domain alone (SAP30BP/ΔN) had no effect on the RBM17 interaction (lower panel). A W257A mutation in the ULM of SAP30BP (SAP30BP/ULMmt), which impairs UHM binding (Pabis et al., 2019), disrupted binding to RBM17 (Figure 3D, lower panel), confirming that the UHM–ULM interaction is critical for the RBM17–SAP30BP complex.

NMR analysis confirmed the RBM17–SAP30BP interaction

To obtain a residue-level resolution mapping of the RBM17–SAP30BP interaction, we performed NMR titration experiments by testing the binding of ^{15}N-labeled RBM17–UHM (RBM17/ΔNΔG) to the C-terminal SAP30BP fragment that harbors the ULM (SAP30BP/ΔNΔH, Figure 4A). Significant amide chemical shift changes confirm the UHM–ULM interaction *via* the RBM17–UHM domain (Figure 4B, Supplementary Figure S4). The most affected area includes the two α-helices and residues close to

the characteristic Arg-Tyr-Phe (RYF) motif (important for ULM binding) of the UHM, indicating a canonical UHM–ULM interaction (Figure 4B, D). Isothermal titration calorimetry (ITC) shows a binding affinity with a dissociation constant K_d = 34.4 μM (Figure 4C). Of note, this is somewhat lower than other reported UHM–ULM interactions (Corsini et al., 2007). In particular, the affinity is about one order of magnitude lower than the interaction of the RBM17–UHM domain with SF3B1–ULM5 (Figure 3C). To analyze which differences in the ULMs of SF3B1 and SAB30BP could explain the reduced affinity, we performed homology modeling based on the known crystal structure of RBM17–UHM bound to SF3B1–ULM5 (Corsini et al., 2007). Considering the sequence similarity of the two ULM sequences, we replaced the ligand by the SAP30BP–ULM (Figure 4D). Analysis of the model complex with the RBM17–UHM and SF3B1–ULM5 indicates that key interactions are preserved, however, with a few exceptions. For example, Arg337 (preceding the important Trp in the SF3B1–ULM) is substituted by Lys256 in SAP30BP (R→K in Figure 3C). While this maintains electrostatic interactions with Asp319 and Glu325 in the RBM17–UHM, hydrogen bond interactions are likely reduced (Figure 4D). Also, the presence of Ser259 in SAP30BP instead of Gln340 in SF3B1 (E→S in Figure 3C) removes a negative charge that interacts with a positively charged region on the surface of the UHM. Taken together, the amino acid differences may rationalize the lower binding affinity of the SAP30BP–ULM. This is consistent with our observation that mechanistically the SF3B1–ULM likely displaces SAP30BP for the binding to the eventual RBM17–UHM.

The GST pull-down assays suggest a contribution of the N-terminal domain of RBM17 in the RBM17–SAP30BP interaction (Figure 3B). We therefore performed additional NMR titration experiments with full-length proteins to identify additional contacts between the two proteins involving the N-terminal regions. To this end, we monitored NMR spectra of three different ^{15}N-labeled constructs upon titration with unlabeled RBM17 variants; SAP30BP/ΔNΔH with RBM17/ΔNΔG, full-length SAP30BP with RBM17/ΔNΔG, and full-length SAP30BP with full-length RBM17 (Figure 4E, left schemata). NMR chemical shift changes of the SAP30BP amide groups were monitored using ^{1}H-^{15}N correlation experiments. The experiments with the full-length constructs confirmed the expected effects for residues in the ULM sequence. However, there were additional spectral changes for residues flanking the ULM

sequence, and in the N-terminal region of SAP30BP upon binding to RBM17 (Figure 4E).

These results, together with the data from the GST pull-down assays, demonstrate that the N-terminal regions of RBM17 and SAP30BP also contribute to the interaction between the two proteins.

RBM17–SAP30BP interaction plays a role to recruit phosphorylated SF3B1

Lastly, we investigated the functional role of the SAP30BP in the context of the following RBM17 binding to SF3B1. Since RBM17 has only one UHM, the RBM17–SAP30BP interaction has to be released prior to the RBM17 interaction with SF3B1 (Figure 1A). This scenario is supported by the stronger binding affinity of RBM17 with SF3B1 compared to that with SAP30BP (see above section). This raises the question: what is the role of the RBM17–SAP30BP interaction? Previously, it was shown that SF3B1 is phosphorylated in the active spliceosome *in vitro* (Wang et al., 1998; Bessonov et al., 2010; Agafonov et al., 2011). SF3B1 phosphorylated at Thr313, mostly localizes in the chromatin fraction, whereas free unphosphorylated SF3B1 is predominantly found in the nucleoplasm (Girard et al., 2012). We therefore postulate that SAP30BP prevents RBM17 binding to inactive unphosphorylated SF3B1 and promotes its binding to active phosphorylated SF3B1.

To examine this hypothesis, we took advantage of an anti-phospho-SF3B1 antibody in our GST pull-down assay (Figure 5A). We found that the depletion of SAP30BP markedly decreased RBM17 binding to phospho-SF3B1 (lanes 4 and 8), indicating that RBM17 alone binds to the excess of unphosphorylated SF3B1, which results in a decrease of the RBM17 association with active phospho-SF3B1. This suggests that a SAP30BP interaction with RBM17 might shield the RBM17–UHM binding surface to prevent binding with inactive free SF3B1–ULM (Figure 6).

To confirm the functional role of an intermediary RBM17–SAP30BP complex, we performed rescue experiments *in vitro* with SAP30BP-depleted HeLa cell extracts supplemented by two recombinant proteins: rSAP30BP and rSAP30BP/ULMmt (Figure 5B). rSAP30BP rescued the binding to phospho-SF3B1 in SAP30BP-depleted extracts, however the rSAP30BP/ULMmt, which hardly bind to RBM17 (Figure 3D), did not (Figure 5B, ‘Pull-Down’ panel; compare with control ‘Buffer’ lane).

We conclude that the intermediary RBM17–SAP30BP complex is important for RBM17 to be recruited to active phosphorylated SF3B1 (Figure 6).

DISCUSSION

SAP30BP was first identified and cloned as HTRP (human transcription regulator protein), which is a cellular co-repressor induced by HSV1 infection and it interacts with SAP30 associated with histone deacetylase complex (HDAC)(Li et al., 2004). The transcriptional co-repressors, SAP30BP and HDAC, interact with BAHCC1 to control the modified histone H3 (H3K27me3)-mediated gene repression (Fan et al., 2020). Here we identified SAP30BP as a functional cofactor of RBM17-dependent splicing in short introns. Therefore SAP30BP adds to the growing list of factors with dual roles in transcription and pre-mRNA splicing. Consistent with our results, a parallel study revealing an important role of murine Sap30bp in promoting splicing of short introns (J. Roth, A.-C. Gingras and B.J. Blencowe, personal communication). Moreover, their results suggested the functional association of Sap30bp in the control of nucleocytoplasmic transport of transcripts associated with the nervous system development.

A novel critical UHM–ULM interaction in RBM17-dependent splicing

UHM–ULM-mediated protein–protein interactions; e.g., U2AF2–SF1, U2AF2–SF3B1, and U2AF1–U2AF2, play essential roles for spliceosome assembly in constitutive splicing (Kielkopf et al., 2001; Selenko et al., 2003; Corsini et al., 2007; reviewed in Loerch and Kielkopf, 2016). UHM–ULM interactions are also involved in alternative splicing regulation; e.g., RBM17–SF3B1 (Corsini et al., 2007), PUF60–SF3B1 (Corsini et al., 2009) and RBM39 (CAPERα)–SF3B1 (Loerch et al., 2014). Recently, we demonstrated that the SF3B1–RBM17 complex (*via* ULM–UHM binding) replaces the SF3B1–U2AF complex (*via* ULM–UHM binding) on the truncated PPT of a subset of short introns (Fukumura et al., 2021).

Here, we discovered a so far unknown ULM–UHM interaction in atypical constitutive splicing targeting short introns. We show that the RBM17–UHM binds to a newly identified ULM in SAP30BP prior to the recruitment of RBM17 to active SF3B1 on pre-

mRNA. The fact that the UHM–ULM interaction in the RBM17–SAP30BP complex is significantly weaker than other UHM–ULM interactions, as demonstrated by our ITC data (Figure 4C), is consistent with a release of SAP30BP from RBM17 upon SF3B1 binding. The SAP30BP–ULM may thus occupy and shield the RBM17–UHM to avoid undesired interactions with other ULMs. And finally, SAP30BP–ULM is replaced by SF3B1–ULM, which has an order of magnitude stronger binding affinity.

The weak and reversible, albeit functional and critical, ULM–UHM interaction between RBM17 and SAP30BP thus provides a unique splicing reaction not known previously.

A conceivable role of RBM17–SAP30BP binding prior to interaction with U2 snRNP

Why does RBM17 need to bind SAP30BP before its interaction with SF3B1 in U2 snRNP? Several data provide clues to address this question. Previous *in vitro* spliceosome analyses demonstrated that SF3B1 is phosphorylated during spliceosome activation, typcally from B to B^{act} complex (Wang et al., 1998; Shi et al., 2006; Bessonov et al., 2010; Agafonov et al., 2011; Hluchý et al., 2022). We therefore paid attention to the phosphorylation status of SF3B1 that interacts with RBM17. Our *in vitro* binding assay revealed that RBM17 can bind to SF3B1 anyway, but without SAP30BP, RBM17 does not bind well to active phosphorylated SF3B1. Importantly, most phosphorylated SF3B1 is present in spliceosomes detected in the chromatin fraction, whereas free unphosphorylated SF3B1 predominantly exists in the nucleoplasmic fraction (Girard et al., 2012). We thus hypothesize that SAP30BP might shield and sequester the UHM domain of RBM17 to prevent its association with free unphosphorylated SF3B1 in the nucleoplasm. And thereby it will ensure that RBM17 can be recruited to active phosphorylated SF3B1 on pre-mRNA (Figure 6).

The composition of spliceosomes and their assembly in RBM17-dependent splicing has not been studied, and thus it is unclear whether the U2 snRNP (SF3B1)–RBM17 complex formation occurs in A complex or the following B complex, as the U2 snRNP (SF3B1)–U2AF interaction occurs in the A complex, and afterwards RBM17 replaces U2AF (Figure 6). In either case, our model suggests that the phosphorylation of SF3B1 for spliceosome activation, in RBM17-dependent splicing occurs somewhat

earlier than in conventional U2AF-dependent splicing. The exact timing of SF3B1 phosphorylation during the RBM17-dependent splicing process remains to be determined. It will also be interesting to investigate if and how phosphorylation of SAP30BP may affect its structural interactions with RBM17 and other binding partners in this process.

3′ splice site recognition in RBM17-dependent splicing

We have not yet identified the responsible factor of the 3′ splice site recognition in the early spliceosomes of RBM17-dependent short introns, such as U2AF1 in U2AF-dependent conventional introns (‘Unknown factor X’ in Figure 6). An involvement of U2AF1 was ruled out by the observation of active RBM17-dependent splicing upon co-depletion of U2AF2 and U2AF1 (Fukumura et al., 2021). Since the RBM17 G-patch motif is critical for RBM17-dependent splicing (Fukumura et al., 2021), we speculate that such a ‘Factor X’, if any, interacts with RBM17 through the G-patch motif to recognize the 3′ splice site. Our ongoing studies aim to identify the putative ‘Factor X’.

The point mutation in the 3′ splice site ‘AG’ has no effects on U2AF-dependent splicing reaction until the first step of splicing in C complex (Gozani et al., 1994; and references therein). Therefore in RBM17-dependent splicing, it is also possible that 3′ splice site recognition may also occur later in the splicing process. We have not yet identified the recognition timing of the 3′ splice site ‘AG’ during the RBM17-dependent splicing cycle.

Previous studies uncovered diversity in recognition of the 3′ splice site. Interestingly, it was reported that excess levels of the SR protein, SRSF2 (SC35), can functionally substitute for U2AF2 in a substrate-specific manner (MacMillan et al., 1997), although the mechanism of this U2AF-independent splicing remains unknown. Indeed, genome-wide analysis of U2AF–RNA interactions suggests that ~12% of functional 3′ splice sites do not require U2AF2 binding or even its function for their recognition (Shao et al., 2014). We are convinced that the 3′ splice sites of the RBM17-dependent introns must be one category of such U2AF2-independent 3′ splice sites.

METHODS

Construction of expression plasmids

The mini-gene plasmids (pcDNA3-AdML, pcDNA3-HNRNPH1 and pcDNA3-EML3), their chimeric variants (pcDNA3-HNRNPH1/AdML-PPT25, pcDNA3-HNRNPH1/AdML-PPT13, pcDNA3-HNRNPH1/5′AdML, pcDNA3-EML3/AdML-PPT25, pcDNA3-EML3/AdML-PPT13 and pcDNA3-EML3/5′AdML), and the RBM17 expression plasmids (pcDNA3-Flag-RBM17, pGEX6p2-RBM17, pGEX6p2-RBM17/ΔG and pGEX6p2-RBM17/UHMmt) were constructed previously (Fukumura et al., 2021; written as 'SPF45' for 'RBM17').

To construct the deleted variants (pGEX6p2-RBM17/ΔN, pGEX6p2-RBM17/ΔN1, pGEX6p2-RBM17/ΔN2, pGEX6p2-RBM17/ΔNΔG pGEX6p2-RBM17/N and pGEX6p2-RBM17/N3), the corresponding ORF regions were PCR-amplified from the parent plasmid pcDNA3-Flag-RBM17 with specific primer sets (Supplementary Table S2) and subcloned into the pGEX6p2 vector (GE Healthcare Life Sciences). To construct the series of SAP30BP and SAP30 expression plasmids (pcDNA3-Myc-SAP30BP, pGEX6p2-SAP30BP, pGEX6p2-SAP30BP/ΔN, pGEX6p2-SAP30BP/ΔC, pGEX6p2-SAP30BP/ΔNΔC and pcDNA3-Myc-SAP30), the corresponding ORF regions were PCR-amplified from HeLa cells cDNA with specific primer sets (Supplementary Table S2) and subcloned into the pcDNA3-Myc or pGEX6p2 vectors (GE Healthcare Life Sciences). Overlap extension PCR was performed to induce the mutation in the ULM of pcDNA3-Myc-SAP30BP (pGEX6p2-SAP30BP/ULMmt).

Expression and purification of recombinant proteins

Various recombinant RBM17 and SAP30BP proteins were expressed from pETM11 vectors with His6-ProteinA TEV cleavable tag using *E. coli* BL21(DE3) in LB medium or in M9 medium supplemented with $^{15}NH_4Cl$ or $^{15}NH_4Cl$ and ^{13}C-D-Glucose. Protein expression was induced at OD_{600} around 0.8–1.0 with 1 mM isopropyl-β-D-thiogalactopyranoside (IPTG), followed by overnight expression at 20°C. Cells were resuspended in 50 mM Tris-HCl (pH 8.0) buffer with 500 mM NaCl, 10 mM imidazole and protease inhibitors, and lysed using French press and sonicator. After centrifugation, the cleared lysates were purified on a Ni-NTA resin column. The

protein samples were further purified by ion exchange chromatography, according to their pI, on a 5 mL HiTrap SP/Q HP column (Cytiva) with 20 mM sodium phosphate (pH 6.5) and by size-exclusion chromatography on a HiLoad 16/60 Superdex 75 column (GE Healthcare Life Sciences) with 20 mM sodium phosphate (pH 6.5) buffer containing 150 mM NaCl. The tag was cleaved with TEV protease and removed with a Ni-NTA column as the final step for SAP30BP/ULM, or before ion exchange chromatography for all other constructs (Figure 4A).

Western blotting analyses

Western blotting was performed as previously described (Fukumura et al., 2021). Briefly, protein samples were boiled with 'NuPAGE LDS Sample Buffer' (Thermo Fisher Scientific), separated by SDS-polyacrylamide gel electrophoresis (SDS-PAGE). The gel was stained with Ponceau S (Cell Signaling Technology), if necessary, and immuno-reactive protein bands were detected by the ECL system and visualized by imaging analyzer (ImageQuant LAS 500, GE Healthcare Life Sciences).

The following commercially available antibodies were used to detect targeted proteins: anti-RBM17 (1:1500 dilution; HPA037478, Sigma-Aldrich), anti-SF3B1 (1:3000 dilution; D221-3, MBL Life Science), anti-Phospho-SF3B1(Thr313)(1:1500 dilution; D8D8V, Cell Signaling Technology), anti-U2AF2 (1:1500 dilution; U4758, Sigma-Aldrich), anti-SAP30BP (1:1500 dilution; HPA052943, Sigma-Aldrich), anti-SAP30 (1:1500 dilution; 27679-1-AP, Proteintech), anti-GAPDH (1:3000 dilution; M171-3, MBL Life Science), anti-Flag (1:3000 dilution; anti-DDDDK tag, M185-3L, MBL Life Science) and anti-cMyc 9E10 antibodies (1:1500 dilution; sc-40, Santa Cruz Biotechnology). Immuno-reactive protein bands were detected by the ECL system and visualized by imaging analyzer (ImageQuant LAS 500, GE Healthcare Life Sciences).

siRNA knockdown and splicing assays

siRNA-mediated knockdown in HeLa cells (ATCC) was performed as previously described (Fukumura et al., 2021). The siRNAs targeting RBM17, SAP30BP and SAP30 were purchased from Fasmac (Supplementary Table S2 for the sequences). At 72 h post-transfection, each protein depletion was checked by Western blotting with

indicated antibodies.

Endogenous splicing products derived from the *HNRNPH1*, *EML3*, *MUS81*, MTA1 and *DUSP1* genes were analyzed by RT–PCR with oligo-dT, random primers and specific primer sets (Supplementary Table S2) as previously described (Fukumura et al., 2021).

To analyze splicing products derived from mini-genes, RBM17- and SAP30BP-depleted HeLa cells were transfected at 48 h post-transfection with 0.5 μg of mini-gene plasmid (Supplementary Table S2) using lipofectamine 2000 reagent (Invitrogen–Thermo Fisher Scientific). These cells were incubated for 24 h prior to the extraction of RNAs described previously (Fukumura et al., 2021). To analyze splicing products from mini-genes, RT–PCR was performed with T7 primer and a specific primer set for each mini-gene (Supplementary Table S2).

All the oligonucleotide primers were purchased from Fasmac (Supplementary Table S2). The PCRs were performed with Blend Taq polymerase (Toyobo Life Science), and the PCR products were analyzed by 6% PAGE and quantified as described previously (Fukumura et al., 2021). All the experiments were independently repeated three times and the means and standard errors of the splicing efficiencies were calculated.

High-throughput RNA sequencing (RNA-Seq) analyses

Six independent total RNAs were prepared by 'NucleoSpin RNA' kit (Macherey-Nagel): these are derived from HeLa cells, treated with two control siRNAs (universal negative control siRNA, Nippon gene), with two RBM17-targeted siRNAs and with two SAP30BP-treated siRNAs. Then enrichment of Poly(A) mRNA was performed with the 'NEBNext Poly(A) mRNA Magnetic Isolation Module' (New England Biolabs). RNA libraries were prepared using the 'NEBNext Ultra Directional RNA Library Prep Kit for Illumina' (New England Biolabs). These samples were sequenced on the high-throughput sequencing platform (NovaSeq6000, Illumina) using a 150 bp paired-end strategy. cDNA library construction and RNA sequencing were performed by a company (Rhelixa).

The sequencing data was analyzed as previously described (Yoshimoto et al., 2021). Obtained sequence reads were mapped onto the human genome reference

sequences (hg19) using the HISAT2 version 2.2.1; the mapped sequence read were assembled using Stringtie version 2.1.7, and the changes of alternative splicing isoforms were analyzed using rMATS version 4.1.1 as previously described (Fukumura et al., 2021). Obtained splicing events were defined as significant changes when the false discovery rate (FDR) was calculated at less than 0.05.

PPT score and length were calculated by SVM-BP finder software as previously described (Yoshimoto et al., 2021). The raw data from the RNA-Seq analysis have been deposited in the SRA database (https://www.ncbi.nlm.nih.gov/sra) under accession number GSE220906.

Immunoprecipitation assays

HeLa cells (in 100-mm dishes) were co-transfected with pcDNA3-Flag-RBM17 and pcDNA3-Myc-SAP30BP (or pcDNA3-Myc-SAP30 as a negative control) using Lipofectamine 2000 reagent (Thermo Fisher Scientific). At 48 h post-transfection, harvested cells were suspended in buffer D [20 mM HEPES-NaOH (pH 7.9), 50 mM KCl, 0.2 mM EDTA, 20% (v/v) glycerol] and sonicated for 20 sec with an ultrasonic disrupter (UR-20P, Tomy Digital Biology). The lysate was centrifuged to remove debris and the supernatant was rocked at 4°C for 2 h with an anti-Flag antibody (anti-DDDDK tag, MBL Life Science) or mouse anti-IgG antibody (Santa Cruz Biotechnology) that was conjugated with 'Dynabeads Protein A' (Veritas) in NET2 buffer [50 mM Tris-HCl (pH7.5), 150 mM NaCl, 0.05% Triton-X100]. The beads were washed five times with NET2 buffer, and the associated proteins were detected by Western blotting (described above) with anti-SF3B1, anti-cMyc, and anti-Flag antibodies.

GST pull-down assays

Recombinant GST-tagged proteins (GST-RBM17, GST-RBM17/ΔN, GST-RBM17/ΔN1, GST-RBM17/ΔN2, GST-RBM17/N, GST-RBM17/N3, GST-RBM17/ΔG, GST-RBM17/ΔNΔG, GST-RBM17/UHMmt, GST-SAP30BP, GST-SAP30BP/ΔN, GST-SAP30BP/ΔC, GST-SAP30BP/ΔNΔC or GST-SAP30BP/ULMmt) were expressed in *E. coli* 'BL21-CodonPlus (DE3)-RIPL' competent cells (Stratagene–Agilent) and purified as previously described (Fukumura et al., 2021). To remove the GST-tag from GST-

SAP30BP proteins (GST-SAP30BP, GST-SAP30BP/ΔN, GST-SAP30BP/ΔC, GST-SAP30BP/ΔNΔC or GST-SAP30BP/ULMmt), 'PreScission Protease' (GE Healthcare Life Sciences) was used according to the manufacturer's protocol.

For *in vitro* binding assays with the recombinant proteins (Figure 3, Supplementary Figure S3), GST-RBM17 variant proteins (20 μg) were mixed with untagged SAP30BP variant proteins (1 μg) in NET2 buffer supplemented with 0.5 mM dithiothreitol (DTT) and incubated at 4°C for 1 h. Then 20 μL of Glutathione Sepharose 4B (GE Healthcare Life Sciences) was added and incubated at 4°C for another 2 h. The incubated beads were washed five times with NET2 buffer and boiled with 'NuPAGE LDS Sample Buffer' to analyze SAP30BP binding by Western blotting with anti-SAP30BP antibody (described above).

For *in vitro* binding assays in HeLa cell extracts (Figure 5), HeLa cells (in 100-mm dishes) were transfected with 500 pmol SAP30BP siRNA or negative control siRNA (Nippon gene) using Lipofectamine RNAi max (Invitrogen–Thermo Fisher Scientific) according to the manufacturer's protocol. At 72 h post-transfection, transfected HeLa cells were suspended in Buffer D and sonicated for 20 sec twice (described above) and centrifuged to remove debris. Obtained siRNA-treated HeLa whole cell extracts (200 μL) were mixed with recombinant GST-RBM17 proteins (20 μg) and incubated at 30°C for 15 min. The SAP30BP or SAP30BP/ULMmt recombinant proteins (1 μg) were added to the above cell extract mixtures to perform rescue experiments (Figure 5B). After RNase A (10 μg, Nippon Gene) treatment at 30°C for 5 min, NET2 buffer was added to a final volume of 500 μL with 20 μL of Glutathione Sepharose 4B and incubated at 4°C for 3 h. The incubated beads were washed five times with NET2 buffer and boiled with 'NuPAGE LDS Sample Buffer' to analyze SF3B1 binding by Western blotting (described above) with indicated antibodies.

NMR spectroscopy

NMR experiments were recorded at 298 K on 500/600/900-MHz Bruker Avance NMR spectrometers equipped with cryogenic triple resonance gradient probes. Backbone ^{1}H, ^{15}N and ^{13}C resonances were assigned with standard triple resonance experiments (HNCO, HN(CA)CO, HNCACB and CBCA(CO)NH described in Sattler et al., 1999). NMR spectra were processed by TOPSPIN3.5 (Bruker) or NMRPipe (Delaglio et al.,

1995) and analyzed using Sparky (T. D. Goddard and D. G. Kneller, SPARKY 3, University of California, San Francisco). Samples were measured at 0.6–0.8 mM protein concentration for triple resonance experiments and 50–100 μM protein concentration for ^{1}H-^{15}N HSQC in NMR buffer [20 mM sodium phosphate (pH 6.5), 150 mM NaCl, 2 mM DTT] with 10% D_2O added as lock signal.

ITC binding analysis

Binding affinities of RBM17/ΔNΔG with SAP30BP/ULM (Figure 4A) were measured using a MicroCal PEAQ-ITC (Malvern Panalytical) in 20 mM sodium phosphate (pH 6.5), 150 mM NaCl at 25°C. RBM17 protein in the cell (concentration ranges, 60–100 μM) was titrated with SAP30BP/ULM (concentration of 800–900 μM) for the final molar ratios of 1:1.7 to 1:3, adjusted depending on the affinity interaction. The standard deviation was determined for 3 replicates.

SUPPLEMENTAL INFORMATION

Supplemental information can be found on the separate file.

ACKNOWLEDGMENTS

We thank Drs. B. Blencowe and Hong Cheng for sharing results prior to publication; Dr. A. R. Krainer for critical reading of the manuscript; H. Shirasaki and T. Kanehisa for technical support; and members of our labs for constructive discussions. We thank Sam Asami and Gerd Gemmecker for support with NMR experiments and acknowledge access to NMR measurements at the Bavarian NMR center in Garching.

K.F. was partly supported by Grants-in-Aid for Scientific Research (C) [Grant number: 18K07304] from the Japan Society for the Promotion of Science (JSPS), a Research Grant from the Hori Sciences and Arts Foundation, and a Research Grant from Nitto Foundation, a Research Grant from Takeda Science foundation, and a Research Grant from Aichi Cancer Research Foundation. A.M. was partly supported by Grants-in-Aid for Scientific Research (B) [Grant number: JP16H04705] and for Scientific Research (C) [Grant number: JP21K06024] from JSPS. L.S. and M.S.

acknowledge support by the Marie Skłodowska-Curie Innovative Training Network (MSCA-ITN) RNAct research of the European Union's Horizon 2020 program [Grant number: 813239]. M.S. acknowledges funding by the Deutsche Forschungsgemeinschaft (DFG, German Research Foundation) with grants [SPP1935 project number 273941853 and SFB1035 project number 201302640].

AUTHOR CONTRIBUTIONS

K.F. and A.M. conceived and designed the experiments; K.F. performed most of the experiments and organized the data; R.Y. performed bioinformatics analyses of the sequencing data; H.-S.K., S.S, L.S. and M.S. performed NMR and ITC experiments and data analysis; A.M. drafted the manuscript and edited the manuscript together with K.F. and M.S. All authors read, corrected and approved the final manuscript. A.M. coordinated and supervised the whole project.

DECLARATION OF INTERESTS

The authors declare no competing interests.

REFERENCES

Agafonov, D.E., Deckert, J., Wolf, E., Odenwalder, P., Bessonov, S., Will, C.L., Urlaub, H., and Lührmann, R. (2011). Semiquantitative proteomic analysis of the human spliceosome via a novel two-dimensional gel electrophoresis method. Mol Cell Biol *31*, 2667–2682.

Behzadnia, N., Golas, M.M., Hartmuth, K., Sander, B., Kastner, B., Deckert, J., Dube, P., Will, C.L., Urlaub, H., Stark, H.*, et al.* (2007). Composition and three-dimensional EM structure of double affinity-purified, human prespliceosomal A complexes. EMBO J *26*, 1737–1748.

Bessonov, S., Anokhina, M., Krasauskas, A., Golas, M.M., Sander, B., Will, C.L., Urlaub, H., Stark, H., and Luhrmann, R. (2010). Characterization of purified human Bact spliceosomal complexes reveals compositional and morphological changes during spliceosome activation and first step catalysis. RNA *16*, 2384–2403.

Corsini, L., Bonnal, S., Basquin, J., Hothorn, M., Scheffzek, K., Valcárcel, J., and Sattler, M. (2007). U2AF-homology motif interactions are required for alternative splicing regulation by SPF45. Nat Struct Mol Biol *14*, 620–629.

Corsini, L., Hothorn, M., Stier, G., Rybin, V., Scheffzek, K., Gibson, T.J., and Sattler, M. (2009). Dimerization and protein binding specificity of the U2AF homology motif of the splicing factor Puf60. J Biol Chem *284*, 630–639.

Delaglio, F., Grzesiek, S., Vuister, G.W., Zhu, G., Pfeifer, J., and Bax, A. (1995). NMRPipe: a multidimensional spectral processing system based on UNIX pipes. J Biomol NMR *6*, 277–293.

Fan, H., Lu, J., Guo, Y., Li, D., Zhang, Z.M., Tsai, Y.H., Pi, W.C., Ahn, J.H., Gong, W., Xiang, Y.*, et al.* (2020). BAHCC1 binds H3K27me3 via a conserved BAH module to mediate gene silencing and oncogenesis. Nat Genet *52*, 1384–1396.

Fukumura, K., Yoshimoto, R., Sperotto, L., Kang, H.S., Hirose, T., Inoue, K., Sattler, M., and Mayeda, A. (2021). SPF45/RBM17-dependent, but not U2AF-dependent, splicing in a distinct subset of human short introns. Nat Commun *12*, 4910.

Girard, C., Will, C.L., Peng, J., Makarov, E.M., Kastner, B., Lemm, I., Urlaub, H., Hartmuth, K., and Lührmann, R. (2012). Post-transcriptional spliceosomes are retained in nuclear speckles until splicing completion. Nat Commun *3*, 994.

Gozani, O., Patton, J.G., and Reed, R. (1994). A novel set of spliceosome-associated proteins and the essential splicing factor PSF bind stably to pre-mRNA prior to catalytic step II of the splicing reaction. EMBO J *13*, 3356–3367.

Hegele, A., Kamburov, A., Grossmann, A., Sourlis, C., Wowro, S., Weimann, M., Will, C.L., Pena, V., Lührmann, R., and Stelzl, U. (2012). Dynamic protein-protein interaction wiring of the human spliceosome. Mol Cell *45*, 567–580.

Herold, N., Will, C.L., Wolf, E., Kastner, B., Urlaub, H., and Lührmann, R. (2009). Conservation of the protein composition and electron microscopy structure of *Drosophila melanogaster* and human spliceosomal complexes. Mol Cell Biol *29*, 281–301.

Hluchý, M., Gajdušková, P., Ruiz de Los Mozos, I., Rájecký, M., Kluge, M., Berger, B.T., Slabá, Z., Potěšil, D., Weiß, E., Ule, J.*, et al.* (2022). CDK11 regulates pre-mRNA splicing by phosphorylation of SF3B1. Nature *609*, 829–834.

Kastner, B., Will, C.L., Stark, H., and Lührmann, R. (2019). Structural Insights into Nuclear pre-mRNA Splicing in Higher Eukaryotes. Cold Spring Harb Perspect Biol *11*, a032417.

Kielkopf, C.L., Rodionova, N.A., Green, M.R., and Burley, S.K. (2001). A novel peptide recognition mode revealed by the X-ray structure of a core $U2AF^{35}/U2AF^{65}$ heterodimer. Cell *106*, 595–605.

Li, J.F., Liu, L.D., Ma, S.H., Che, Y.C., Wang, L.C., Dong, C.H., Zhao, H.L., Liao, Y., and Li, Q.H. (2004). HTRP–an immediate-early gene product induced by HSV1 infection in human embryo fibroblasts, is involved in cellular co-repressors. J Biochem *136*, 169–176.

Loerch, S., and Kielkopf, C.L. (2016). Unmasking the U2AF homology motif family: a bona fide protein-protein interaction motif in disguise. RNA *22*, 1795–1807.

Loerch, S., Maucuer, A., Manceau, V., Green, M.R., and Kielkopf, C.L. (2014). Cancer-relevant splicing factor CAPERα engages the essential splicing factor SF3b155 in a specific ternary complex. J Biol Chem *289*, 17325–17337.

López-Mejía, I., and Tazi, J. (2012). In vivo analysis of splicing assays. In Alternative pre-mRNA splicing: Theory and protocols, S. Stamm, C. Smith, and R. Lührmann, eds. (Weinheim, Germany: Wiley-Blackwell), pp. 392–399.

MacMillan, A.M., McCaw, P.S., Crispino, J.D., and Sharp, P.A. (1997). SC35-mediated reconstitution of splicing in U2AF-depleted nuclear extract. Proc Natl Acad Sci USA *94*, 133–136.

Mayeda, A., and Krainer, A.R. (2012). In vitro splicing assays. In Alternative pre-mRNA splicing: Theory and protocols, S. Stamm, C. Smith, and R. Lührmann, eds. (Weinheim, Germany: Wiley-Blackwell), pp. 321–329.

Pabis, M., Corsini, L., Vincendeau, M., Tripsianes, K., Gibson, T.J., Brack-Werner, R., and Sattler, M. (2019). Modulation of HIV-1 gene expression by binding of a ULM motif in the Rev protein to UHM-containing splicing factors. Nucleic Acids Res *47*, 4859–4871.

Piovesan, A., Caracausi, M., Ricci, M., Strippoli, P., Vitale, L., and Pelleri, M.C. (2015). Identification of minimal eukaryotic introns through GeneBase, a user-friendly tool for parsing the NCBI Gene databank. DNA Res *22*, 495–503.

Sattler, M., Schleucher, J., and Griesinger, C. (1999). Heteronuclear multidimensional NMR experiments for the structure determination of proteins in solution employing pulsed field gradients. Prog Nucl Magn Reson Spectrosc *34*, 93–158.

Selenko, P., Gregorovic, G., Sprangers, R., Stier, G., Rhani, Z., Kramer, A., and Sattler, M. (2003). Structural basis for the molecular recognition between human splicing factors U2AF65 and SF1/mBBP. Mol Cell *11*, 965–976.

Shao, C., Yang, B., Wu, T., Huang, J., Tang, P., Zhou, Y., Zhou, J., Qiu, J., Jiang, L., Li, H.*, et al.* (2014). Mechanisms for U2AF to define 3' splice sites and regulate alternative splicing in the human genome. Nat Struct Mol Biol *21*, 997–1005.

Shi, Y., Reddy, B., and Manley, J.L. (2006). PP1/PP2A phosphatases are required for the second step of pre-mRNA splicing and target specific snRNP proteins. Mol Cell *23*, 819–829.

Wang, C., Chua, K., Seghezzi, W., Lees, E., Gozani, O., and Reed, R. (1998). Phosphorylation of spliceosomal protein SAP 155 coupled with splicing catalysis. Genes Dev *12*, 1409–1414.

Will, C.L., and Lührmann, R. (2011). Spliceosome structure and function. Cold Spring Harb Perspect Biol *3*, a003707.

Yoshimoto, R., Chhipi-Shrestha, J.K., Schneider-Poetsch, T., Furuno, M., Burroughs, A.M., Noma, S., Suzuki, H., Hayashizaki, Y., Mayeda, A., Nakagawa, S.*, et al.* (2021). Spliceostatin A interaction with SF3B limits U1 snRNP availability and causes premature cleavage and polyadenylation. Cell Chem Biol *28*, 1356–1365 e1354.

FIGURES

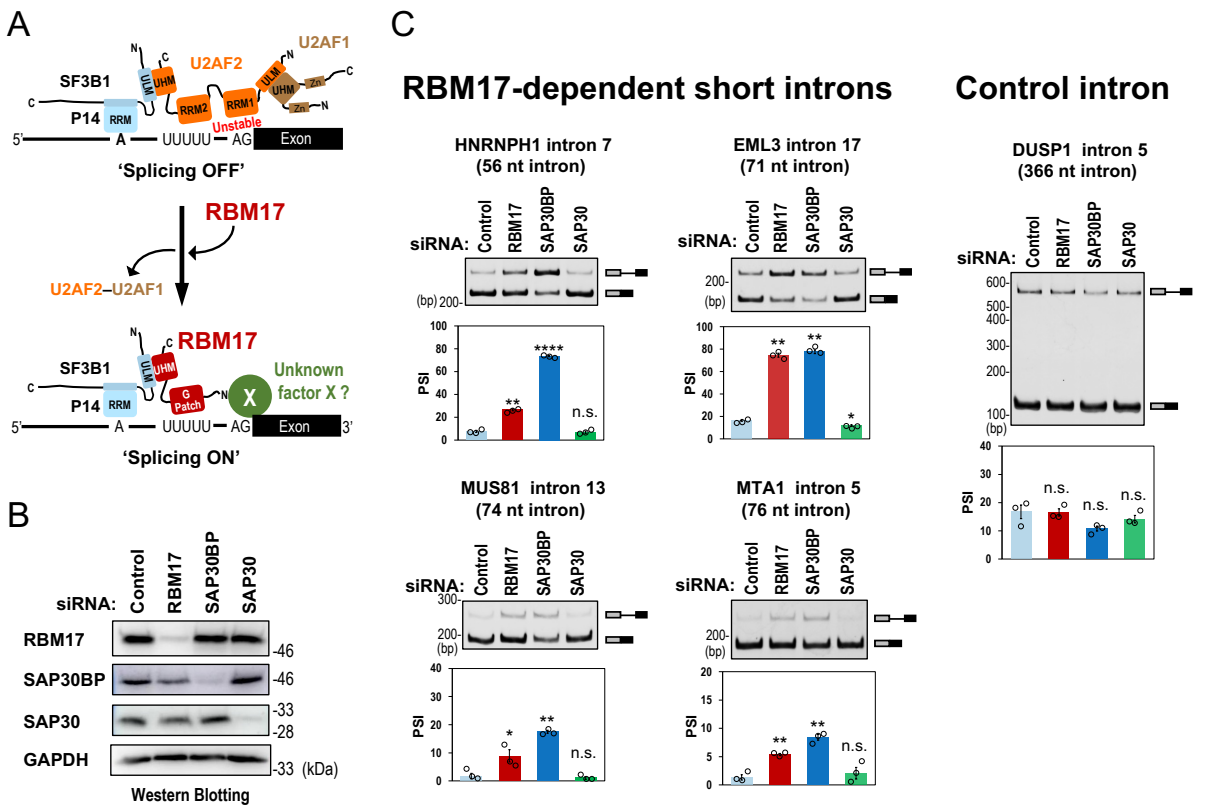

Figure 1. SAP30BP is additionally required for RBM17-dependent splicing of pre-mRNAs with short introns

(A) The model of RBM17-dependent splicing on a short intron with a truncated PPT (indicated by UUUUU)(Fukumura et al., 2021). The associated splicing factors with the domain structures and the target sequences of pre-mRNAs are represented schematically. 'Unknown factor X' was postulated in this study.

(B) The depletion of RBM17, SAP30BP, SAP30 proteins by siRNA-knockdown in HeLa cells. The depleted proteins were checked by Western blotting with indicated antibodies.

(C) *In cellulo* splicing assays of the pre-mRNAs including indicated introns. After the indicated siRNA transfection in HeLa cells, endogenous splicing of the four RBM17-dependent short introns and one RBM17-independent control intron were analyzed by RT–PCR. Means ± SEM are given for three independent experiments and two-tailed paired Student *t*-test values were calculated (**P* < 0.05, ***P* < 0.01, *****P* < 0.0001, $^{n.s.}$ *P* > 0.05).

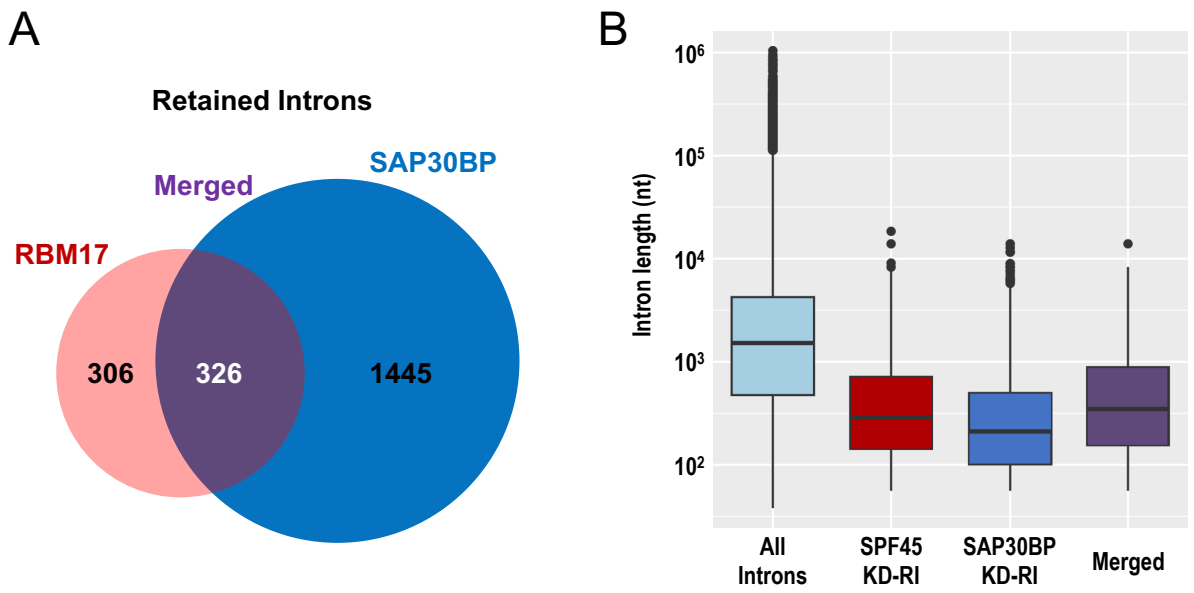

Figure 2. RBM17 and SAP30BP are generally required for the splicing of pre-mRNAs including short introns

(A) Venn diagram for significantly retained introns upon siRNA-knockdown of RBM17 and SAP30BP in HeLa cells.

(B) Box-plots for the intron-length distributions of all introns in human RefGene and the retained introns (RI) in RBM17- and SAP30BP-knockdown (KD) HeLa cells. Box-plots indicate the summary of the dataset; median (middle line), 25–75th percentile (box), and <5th and >95th percentile (whiskers), together with outliers (single points).

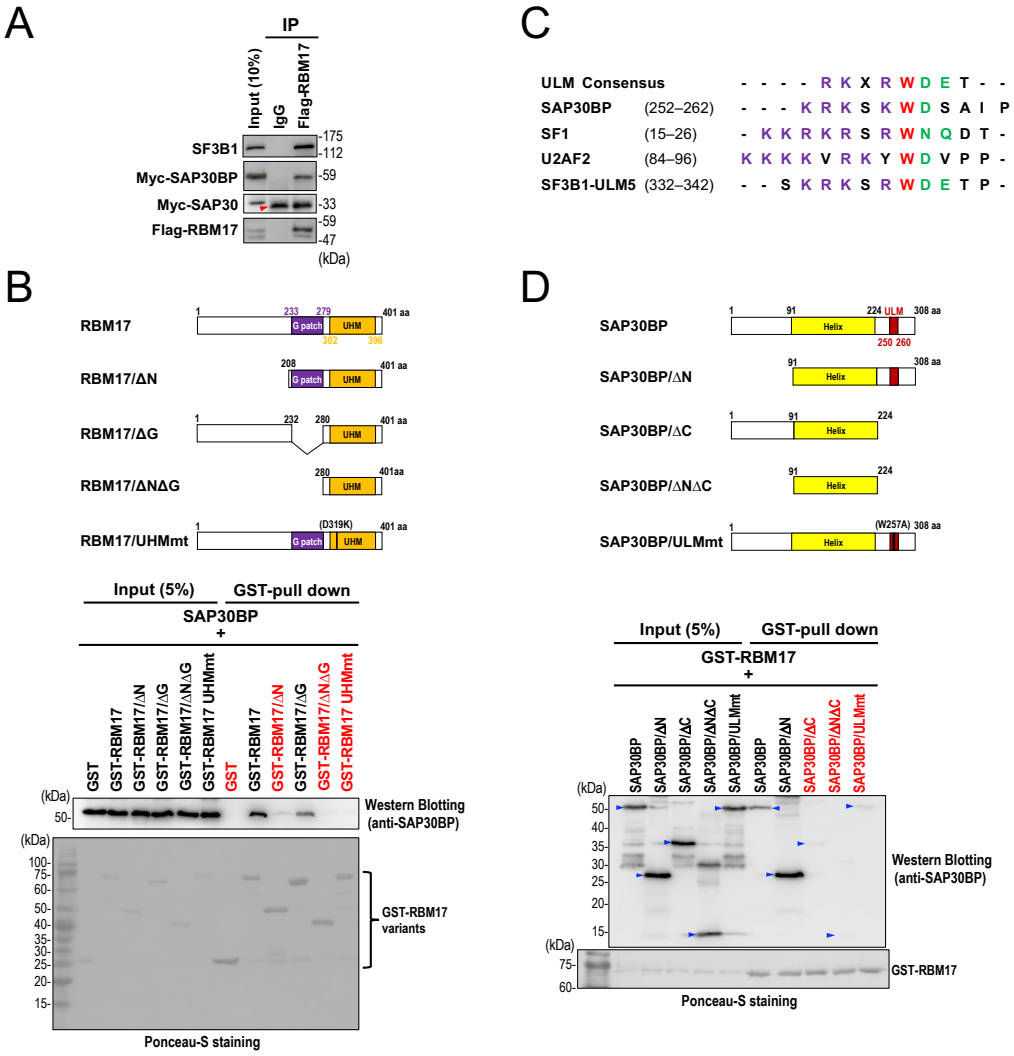

Figure 3. UHM in RBM17 and newly found ULM in SAP30BP are critical for the binding between RBM17 and SAP30BP

(A) Co-immunoprecipitation of RBM17 with SAP30BP and SF3B1. HeLa cells were co-transfected with Myc-SAP30BP, Myc-SAP30 (negative control) and Flag-RBM17 plasmids, these transfected cell extracts were immunoprecipitated using mouse IgG or anti-Flag antibody, and the immunoprecipitated proteins were analyzed by Western blotting. The red arrow head indicates IgG light chain of anti-Flag antibody.

(B) *In vitro* GST-pulldown assay (after RNase A-treatment) to detect the direct binding between indicated RBM17 variant proteins and SAP30BP protein. Red-colored variants indicate the diminished protein binding with SAP30BP. Recombinant SAP30BP protein associated with these GST-fused proteins was detected by Western blotting using anti-SAP30BP antibody. The same membrane was also stained with ponceau S to evaluate the loading amount and the comparable precipitation of the GST or GST fusion proteins.

(C) Alignment of ULM sequences in SAP30BP, SF1, U2AF2 and SF3B1 (ULM5) with the ULM consensus sequence. Conserved amino acid residues are denoted by colors: PURPLE–basic residues preceding the conserved tryptophan (W); RED–conserved W; GREEN–acidic and N/Q-type residues following the conserved W.

(D) *In vitro* GST-pulldown assay (with RNase A-treatment) to detect the direct binding between indicated SAP30BP variants (indicated by blue arrow heads) and RBM17. Red-colored variants indicate the diminished protein binding with RBM17. See (B) for the methods.

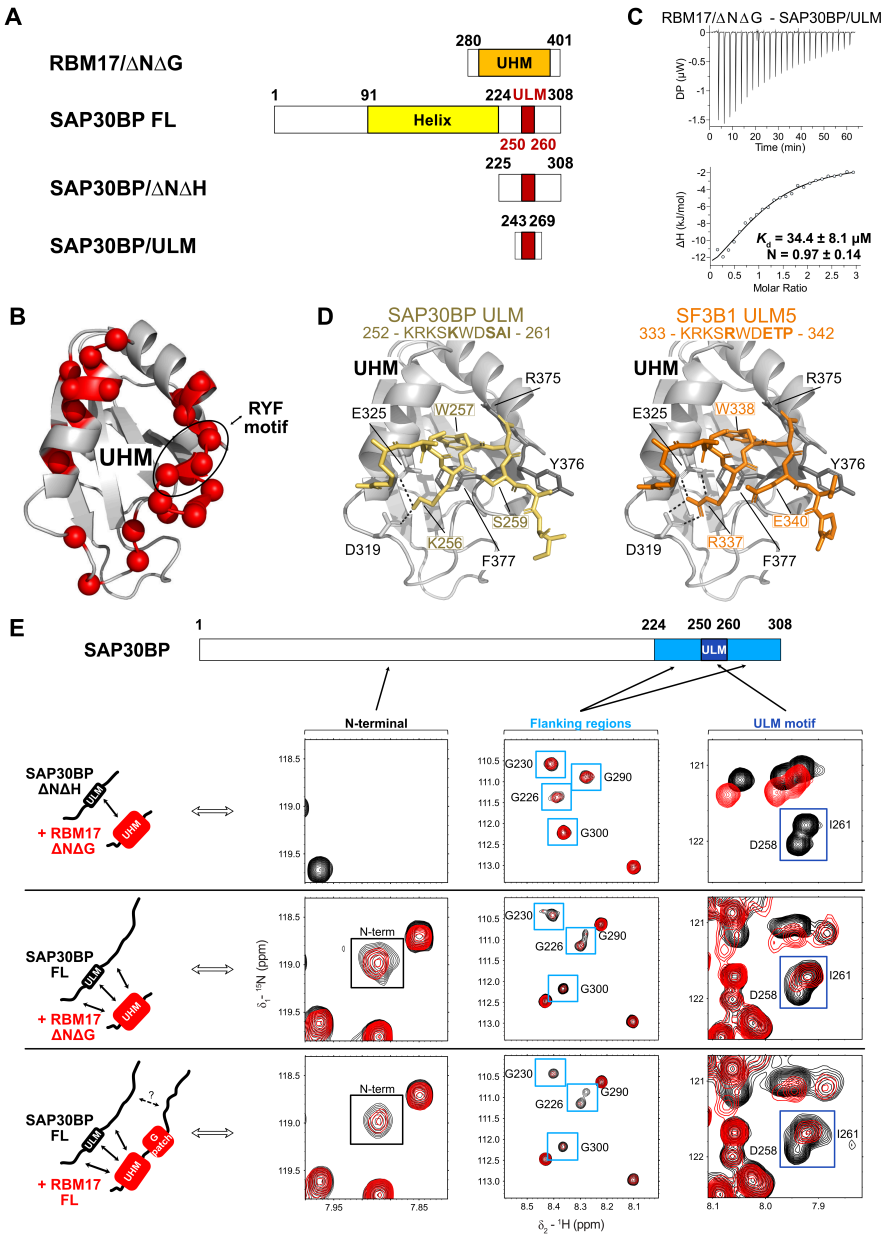

Figure 4. The RBM17–SAP30BP interaction was confirmed by NMR and Isothermal titration calorimetry (ITC)

(A) RBM17 and SAP30BP variant constructs used for NMR and ITC experiments.

(B) NMR chemical shift perturbation (>0.65 ppm) of RBM17/ΔNΔG, upon adding 6-fold molar excess of SAP30BP/ΔNΔH, is highlighted on RBM17–UHM structure (red spheres). The position of the Arg-Tyr-Phe (RYF)-motif is indicated.

(C) ITC binding analysis (isotherm) of RBM17/ΔNΔG and SAP30BP/ULM.

(D) Crystal structure of SF3B1–ULM5 bound to RBM17–UHM (right, PDB accession code 2PEH) and homology model of the SAP30BP–ULM peptide bound to the RBM17–UHM (left). Differences in amino acid sequences are shown in bold. The RYF motif (R375-Y376-F377) of RBM17–UHM and other key interface residues are labelled.

(E) Comparison of ^{1}H-^{15}N HSQC spectra of SAP30BP (ΔNΔH or full-length, in black) upon addition of RBM17 (ΔNΔG or full-length, in red), corresponding to the schemata (left). Representative resonances belonging to the N-terminal (left, black square), flanking (middle, cyan square), and ULM (right, blue square) regions in SAP30BP are displayed.

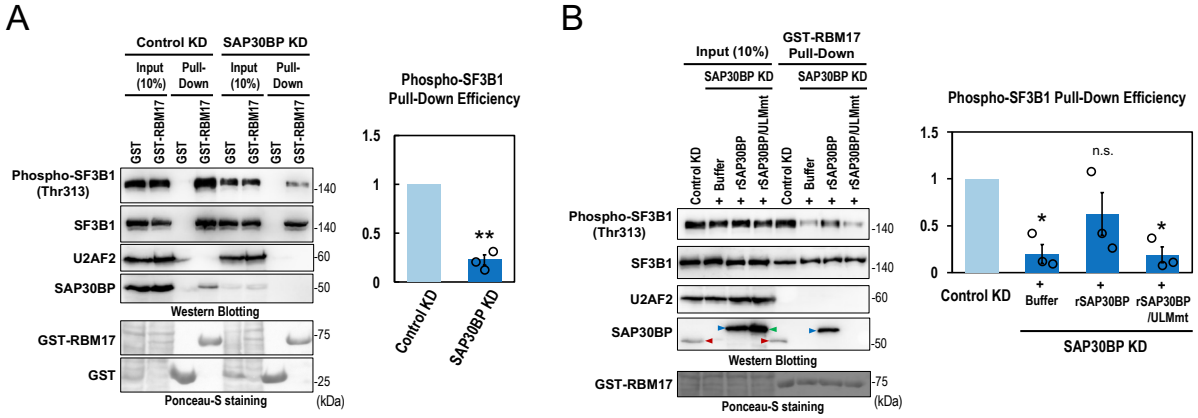

Figure 5. Binding of RBM17 to SAP30BP is critical for RBM17 to be recruited in active phospho-SF3B1

(A) Binding of RBM17 to total SF3B1 and phosphorylated SF3B1 under SAP30bp-depletion. GST pull-down assay with whole cell extracts prepared from SAP30BP-knockdown HeLa cells. Proteins associated with GST-RBM17 protein were detected by Western blotting using the indicated antibodies. Membrane was also stained with ponceau S for loading and precipitation controls. The bar graph shows quantification of the bands on Western blots. Phospho-SF3B1 scanned data were normalized to SF3B1 (Phospho-SF3B1/SF3B1) and plotted. Means ± SEM are given for four independent experiments and two-tailed Student t-test values were calculated (**$P < 0.01$, *$P < 0.05$, $^{n.s.}$ $P > 0.05$).
(B) Rescue experiments of diminished RBM17–phospho-SF3B1 binding under SAP30BP-depletion. The same reaction mixtures in panel (A) were supplemented with recombinant SAP30BP or SAP30BP/ULMmt proteins and the associated proteins with GST-RBM17 were analyzed by Western blotting with indicated antibodies. See (A) for plotted scanned data and the statistical analysis.

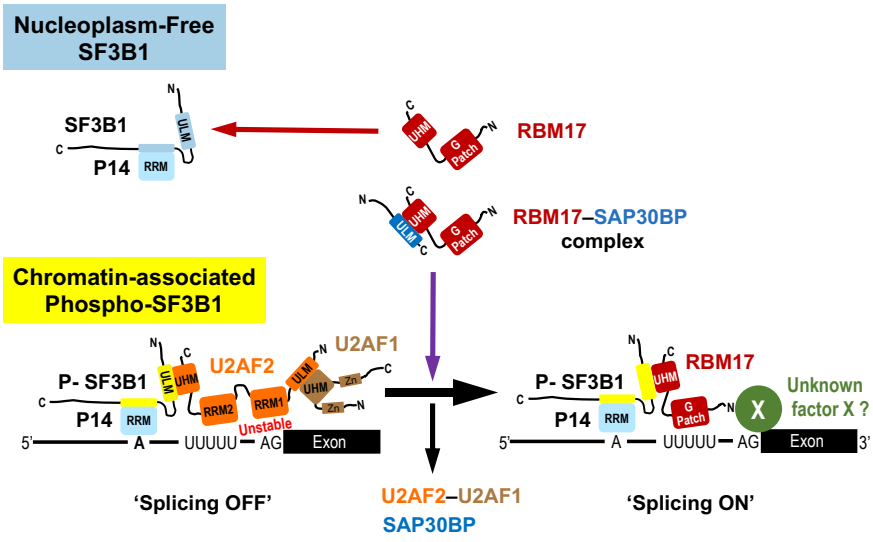

Figure 6. The model of RBM17–SAP30BP complex-dependent splicing on a short intron with a truncated PPT. RBM17 alone can bind with free unphosphorylated SF3B1 in the nucleoplasm, while intermediary RBM17–SAP30BP complex prevents this non-functional binding, which allows functional RBM17 binding to active phosphorylated SF3B1 on pre-mRNA. The associated splicing factors with the domain structures and the target sites of pre-mRNAs are represented schematically.

SAP30BP interacts with RBM17/SPF45 to promote splicing in a subset of human short introns

Kazuhiro Fukumura[1]*, Luca Sperotto[2,3], Stefanie Seuß[2,3], Hyun-Seo Kang[2,3], Rei Yoshimoto[4], Michael Sattler[2,3], and Akila Mayeda[1,5]*

[1]Division of Gene Expression Mechanism, Center for Medical Science, Fujita Health University, Toyoake, Aichi 470-1192, Japan
[2]Institute of Structural Biology, Helmholtz Zentrum München, 85764 Neuherberg, Germany
[3]Bavarian NMR Center, School of Natural Sciences, Technical University of Munich, 85748 Garching, Germany
[4]Department of Applied Biological Sciences, Faculty of Agriculture, Setsunan University, Hirakata, Osaka 673-0101, Japan

[5]Lead contact
*Correspondences: fukumura@fujita-hu.ac.jp (K.F.), mayeda@fujita-hu.ac.jp (A.M.)

Contents

Table S1
(Uploaded in a separate PDF file)

Table S2

Figure S1

Figure S2

Figure S3

Figure S4

Table S2. List of synthetic oligonucleotides used in the experiments

siRNAs (sense sequences) for cellular knockdown (dT: deoxyribonucleotide)		
SPF45-siRNA	5′- GACCCUAUGUUUCCUAAUGdTdT-3′	Knockdown of SPF45
SAP30BP-siRNA	5′- GAGAAAGGCGGAUUGGUAUdTdT-3′	Knockdown of SAP30BP
SAP30-siRNA	5′- GUUCGAAACAGAAGAAAGAdTdT-3′	Knockdown of SAP30
Primer DNAs for plasmid constructions		
SPF45/ΔN infusion F	5′-CAGTGTGCTGGAATTCTGGCCATTCCTCCCCCAGTG-3′	Construction of pGEX6p2-SPF45/ΔN
SPF45 infusion R	5′-TAGATGCATGCTCGAGTCAAACTTGTTCTGCCAAATCC-3′	
SPF45/ΔN1 infusion F	5′-CAGTGTGCTGGAATTCTGGACCCTATGTTTCCTAATGAT-3′	Construction of pGEX6p2-SPF45/ΔN1
SPF45-R-infusion R	5′-TAGATGCATGCTCGAGTCAAACTTGTTCTGCCAAATCC-3′	
SPF45 infusion F	5′-CAGTGTGCTGGAATTCTGATGTCCCTGTACGATGACCT -3′	Construction of pGEX6p2-SPF45/ΔN2
SPF45/ΔN2 R	5′-ATGGCATCATTAGGAAACATAGGGTCATATTCG-3′	
SPF45/ΔN2 F	5′-ATGTTTCCTAATGATGCCATTCCTCCCCCAGTG-3′	
SPF45 infusion R	5′-TAGATGCATGCTCGAGTCAAACTTGTTCTGCCAAATCC-3′	
SPF45 infusion F	5′-CAGTGTGCTGGAATTCTGATGTCCCTGTACGATGACCT-3′	Construction of pGEX6p2-SPF45/N
SPF45/N infusion R	5′-TAGATGCATGCTCGAGTCAAGCGAGGAAGGAGTTG-3′	
SPF45/N3 infusion F	5′-CAGTGTGCTGGAATTCTGCTCGCCCCAGTCATTGA-3′	Construction of pGEX6p2-SPF45/N3
SPF45/N3 infusion R	5′-TAGATGCATGCTCGAGTCATCTCCTTGCAAACCCA-3′	
SPF45/ΔNΔG infusion F	5′-CAGTGTGCTGGAATTCTGGGCGACGCCACAGAGAAA-3′	Construction of pGEX6p2-SPF45/ΔNΔG
SPF45 infusion R	5′-TAGATGCATGCTCGAGTCAAACTTGTTCTGCCAAATCC-3′	
SAP30BP infusion F	5′-CAGTGTGCTGGAATTCTGATGGCGGGGAAGAAGAATGT-3′	Construction of pcDNA3-Myc-SAP30BP& pGEX6p2-SAP30BP
SAP30BP infusion R	5′-TAGATGCATGCTCGAG TCACTGCTTGGCCTTCTTCA-3′	
SAP30BP/ΔN infusion F	5′-CAGTGTGCTGGAATTCTGACAGAAGCAGAAAAGCGAGACC-3′	Construction of pGEX6p2-SAP30BP/ΔN
SAP30BP infusion R	5′-TAGATGCATGCTCGAGTCACTGCTTGGCCTTCTTCA-3′	
SAP30BP infusion F	5′-CAGTGTGCTGGAATTCTGATGGCGGGGAAGAAGAATGT-3′	Construction of pGEX6p2-SAP30BP/ΔC
SAP30BP/ΔC infusion R	5′-TAGATGCATGCTCGAGTCACACAAACTCAATTTTTGTTCGCTC-3′	
SAP30BP/ΔN infusion F	5′-CAGTGTGCTGGAATTCTGACAGAAGCAGAAAAGCGAGACC-3′	Construction of pGEX6p2-SAP30BP/ΔNΔC
SAP30BP/ΔC infusion R	5′-TAGATGCATGCTCGAGTCACACAAACTCAATTTTTGTTCGCTC-3′	
SAP30BP infusion F	5′-CAGTGTGCTGGAATTCTGATGGCGGGGAAGAAGAATGT-3′	Construction of pGEX6p2-SAP30BP/ULMmt
SAP30BP ULMmt-W257A R	5′-GCCGAATCCGCCTTGCTCTTTCTCTTCTGAGC-3′	
SAP30BP ULMmt-W257A F	5′-AGAGCAAGGCGGATTCGGCTATCCCAGTGA-3′	
SAP30BP infusion R	5′-TAGATGCATGCTCGAG TCACTGCTTGGCCTTCTTCA-3′	
SAP30 infusion F	5′-CAGTGTGCTGGAATTCTGATGAACGGCTTCACGCCTG-3′	Construction of pcDNA3-Myc-SAP30
SAP30 infusion R	5′-TAGATGCATGCTCGAGCTAGTGAACACCACTATCAACCTTG-3′	
Primer DNAs for analysis		
HNRNPH1-E7F-EcoRI	5′-GGAATTCCGCTATGGAGGCTATGATGA-3′	Splicing assay of endogenous HNRNPH1 intron 7
HNRNPH1-E8R-XhoI	5′-CCCTCGAGGGCAGTAGCTCTGTAAGGTAAT-3′	
EML3-E17F-EcoRI	5′-GGAATTCCGTGGTTGGTTTTGGACACAG-3′	Splicing assay of endogenous EML3 intron 17
EML3-E18R-XhoI	5′-CCCTCGAGGGCATACAGCGGCCAAAGCGGC-3′	
MUS81-E13F-EcoRI	5′-GGAATTCCCCCTGGGAACCCTGAATCAG-3′	Splicing assay of endogenous MUS81 intron 13
MUS81-E14R-XhoI	5′-CCGCTCGAGGGTGCTGTATCGATCCACCA-3′	
MTA1-E5F-EcoRI	5′-GGAATTCCGAAATGGAGAACCCGGAAATG-3′	Splicing assay of endogenous MTA1 intron 5
MTA1-E6R-XhoI	5′-CCGCTCGAGGCTCCAGGTAGGACTTGAG-3′	
DUSP1-F	5′-TGCAGTACCCCACTCTACGA-3′	Splicing assay of endogenous DUSP1 intron 2
DUSP1-R	5′-GAGACGTTGATCAAGGCAGTG-3′	
T7	5′-AATACGACTCACTATAG-3′	Splicing assay of AdML mini-gene pre-mRNA
AdML-E2R	5′-ACCGCGAAGAGTTTGTCCTCAACC-3′	
T7	5′-AATACGACTCACTATAG-3′	Splicing assay of HNRNPH1 mini-gene pre-mRNA
HNRNPH1-E8R-XhoI	5′-CCCTCGAGGGCAGTAGCTCTGTAAGGTAAT-3′	
T7	5′-AATACGACTCACTATAG-3′	Splicing assay of EML3 mini-gene pre-mRNA
EML3-E1R-XhoI	5′-CCCTCGAGGGCATACAGCGGCCAAAGCGGC-3′	

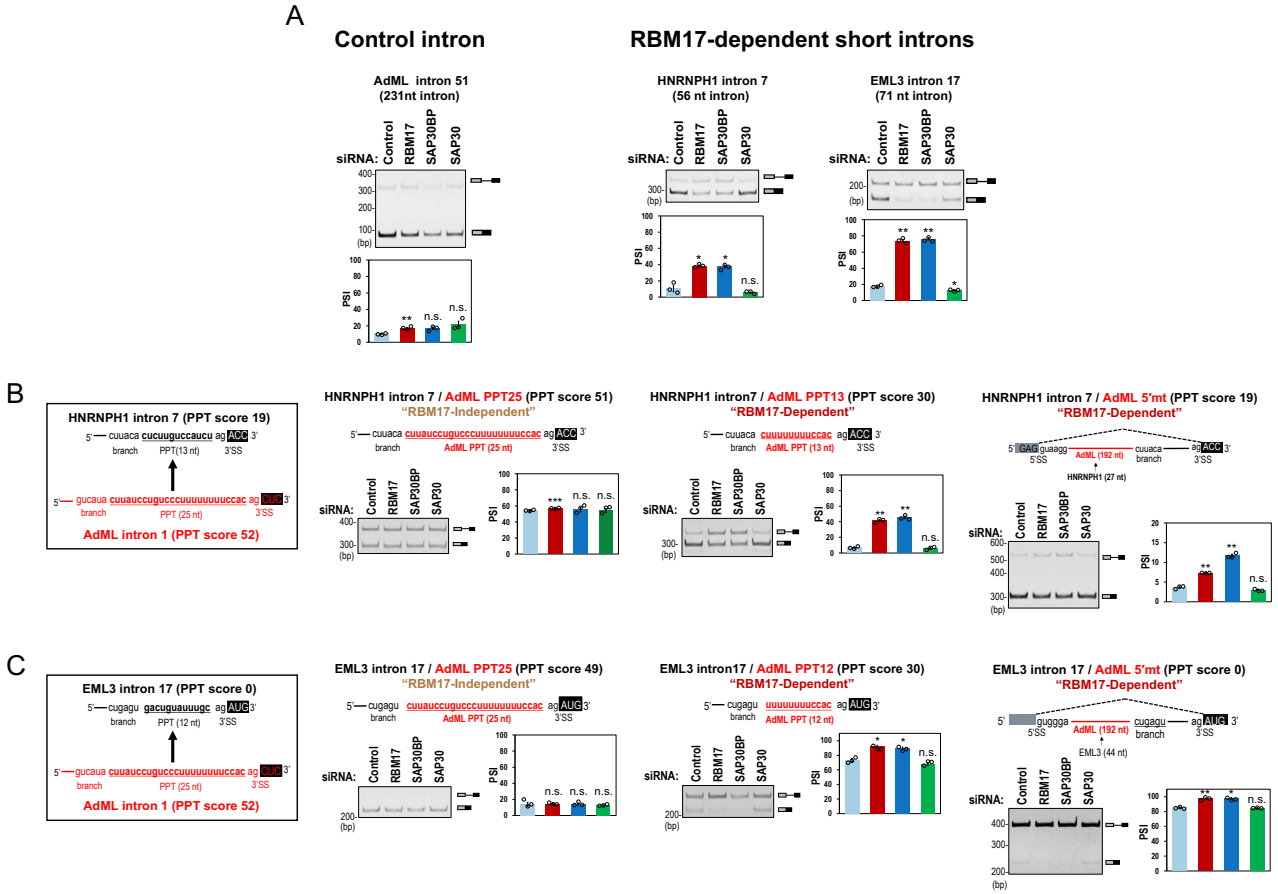

Figure S1. The length of poly-pyrimidine tracts (PPTs) determine the co-dependency of RBM17 and SAP30BP in splicing

(A) Selectively repressed splicing of pre-mRNAs with short introns in RBM17- and SAP30BP-depleted cells. Indicated three pre-mRNAs were expressed from mini-genes in HeLa cells treated with RBM17, SAP30BP or SAP30 (negative control) siRNA and their splicing was assayed by RT–PCR. PAGE images and graphs of PSI (percent spliced in) values are shown. Means ± SEM are given for three independent experiments and two-tailed Student *t*-test values were calculated (**P* < 0.05, ***P* < 0.01, ****P* < 0.001, n.s. *P* > 0.05).

(B, C) Selectively repressed splicing of the chimeric HNRNH1 and EML3 pre-mRNAs with truncated PPT in RBM17- and SAP30BP-depleted cells. These chimeric pre-mRNAs are schematically shown (red color indicates AdML derived sequences). The PPT score (see Methods) is one of the criteria to evaluate effective PPTs. See (A) for *in cellulo* splicing assay and the statistical analysis.

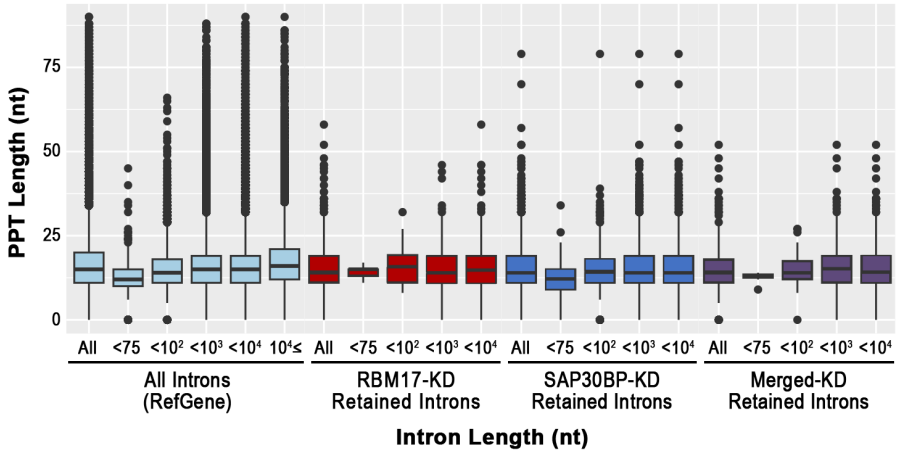

Figure S2. Truncated polypyrimidine tract (PPT) is dominated in introns shorter than 75 nt.
The box plots show the similar PPT-length distributions of all introns (in human RefGene) with those of the retained introns in RBM17- and SAP30BP-knockdown HeLa cells, suggesting that shorter introns generally tend to possess the shorter PPTs. The same analysis in RBM17-knockdown HEK293 cells were described previously (Fukumura et al. 2021; see References in the text), in which PPT lengths of RBM17-dependent short introns were shorter than those of the whole RefGene introns. Box plots show the summary of the data set; median (middle line), 25–75th percentile (box), and <5th and >95th percentile (whiskers), together with outliers (single points).

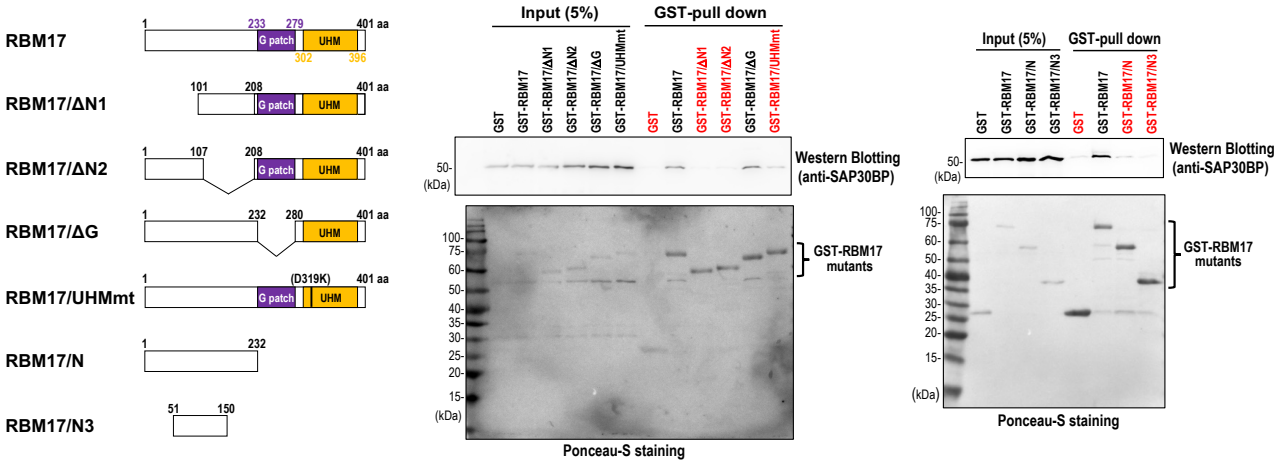

Figure S3. UHM and full N-terminal region in RBM17 are important for the SAP30BP binding
Direct interaction of RBM17 mutants with SAP30BP, as shown by immunoblot analysis of the *in vitro* GST-pulldown assay for purified GST, GST-RBM17/DG, RBM17/UHMmt,GST-RBM17/DN1, GST-RBM17/DN2 or RBM17/N of RBM17/N3 with purified SAP30BP. Membrane was also stained by ponceau S to show the general loading as well as the comparable precipitation of the GST or GST fusion proteins.

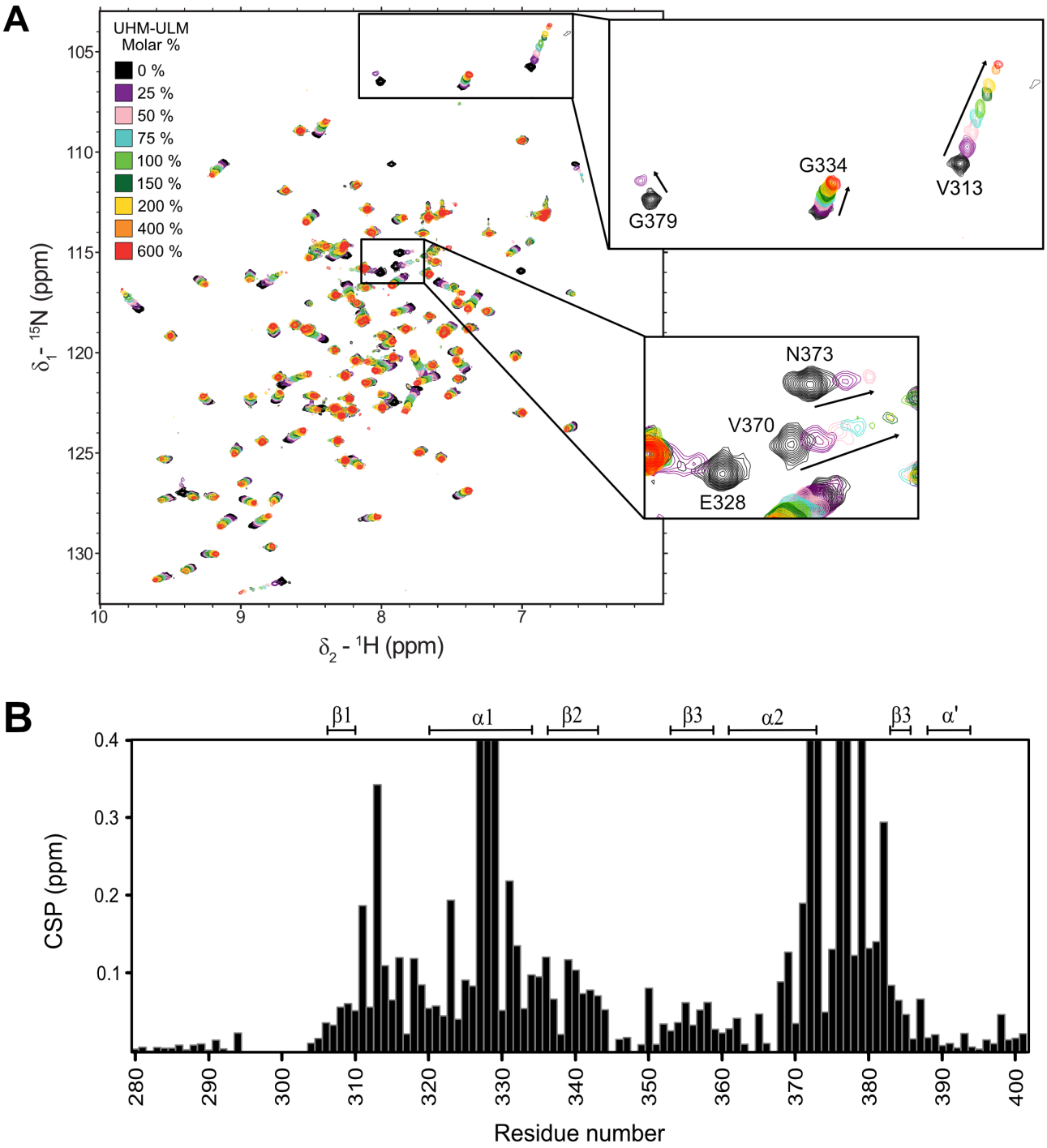

Figure S4. NMR spectral changes reveal the interaction between the RBM17–UHM and SAP30BP–ULM

(A) 1H-15N HSQC spectra of RBM17–UHM domain (RBM17/ΔNΔG) upon titration with SAP30BP–ULM domain (SAP30BP/ΔNΔH).

(B) Bar plot of the calculated chemical shift perturbation observed in the spectrum in panel A. The secondary structure of the RBM17 UHM domain is indicated on top.